Stochastic simulations of classical PDEs with non-trivial boundary conditions

Magnus Ögren

School of Science and Technology

Örebro University, Sweden

2019-09-30

Why did I start with this research… Background:

Computer Physics Communications 182 (2011) 1999–2003

Contents lists available at ScienceDirect

Computer Physics Communications

www.elsevier.com/locate/cpc

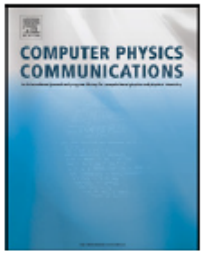

Stochastic simulations of fermionic dynamics with phase-space representations

M. Ögren *, K.V. Kheruntsyan, J.F. Corney

ARC Centre of Excellence for Quantum-Atom Optics, School of Mathematics and Physics, University of Queensland, Brisbane, Queensland 4072, Australia

simulation. For Hamiltonians containing up to four operators, a second-order partial differential equation is generated, which can be written in the form of a Fokker–Planck equation (FPE):

$$\frac{d}{dt}P(\vec{\lambda}) = \left[-\sum_j \frac{\partial}{\partial\lambda_j}A_j(\vec{\lambda}) + \frac{1}{2}\sum_{j,k}\frac{\partial^2}{\partial\lambda_j\partial\lambda_k}D_{ij}(\vec{\lambda})\right]P(\vec{\lambda}). \qquad (5)$$

a mapping [14,15] to an equivalent set of stochastic differential equations (SDEs) to sample the moments of the distribution. In the Itō calculus, stochastic equations corresponding to Eq. (6) have the general form

$$\begin{aligned}
dn_{\mathbf{k}} &= \left(\alpha m_{\mathbf{k}}^{+} + \alpha^{+} m_{\mathbf{k}}\right)d\tau + N_0^{-1/2}\mathbf{B}^{(n_{\mathbf{k}})}\,\mathbf{dW},\\
dm_{\mathbf{k}} &= \left[-2i\delta_{\mathbf{k}}m_{\mathbf{k}} + \alpha(1-2n_{\mathbf{k}})\right]d\tau + N_0^{-1/2}\mathbf{B}^{(m_{\mathbf{k}})}\,\mathbf{dW},\\
dm_{\mathbf{k}}^{+} &= \left[2i\delta_{\mathbf{k}}m_{\mathbf{k}}^{+} + \alpha^{+}(1-2n_{\mathbf{k}})\right]d\tau + N_0^{-1/2}\mathbf{B}^{(m_{\mathbf{k}}^{+})}\,\mathbf{dW},\\
d\alpha &= -\frac{1}{N_0}\sum_{\mathbf{k}} m_{\mathbf{k}}\,d\tau + N_0^{-1/2}\mathbf{B}^{(\alpha)}\,\mathbf{dW},\\
d\alpha^{+} &= -\frac{1}{N_0}\sum_{\mathbf{k}} m_{\mathbf{k}}^{+}\,d\tau + N_0^{-1/2}\mathbf{B}^{(\alpha^{+})}\,\mathbf{dW}, \qquad (7)
\end{aligned}$$

Why did I start with this research…
Given a task (from funder!):

Understand properties of large rocks from small samples…

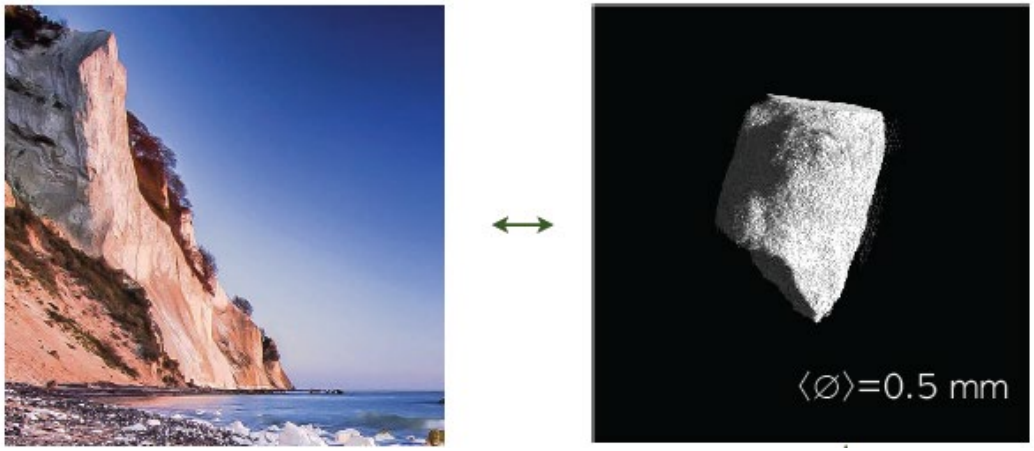

Data from synchrotron radiation facilities.

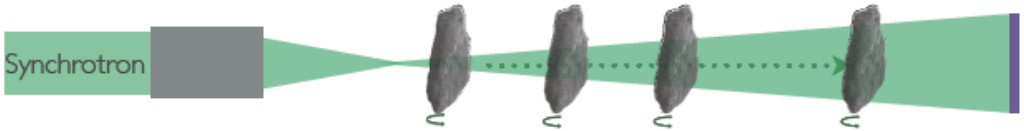

Measurement done at different positions in the conical beamline gives different resolution.

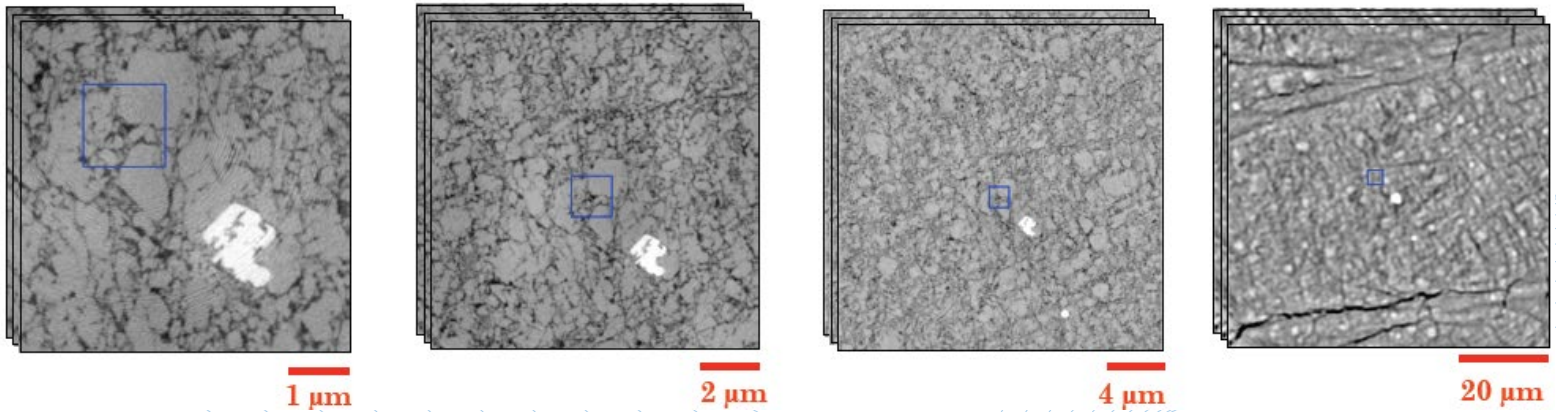

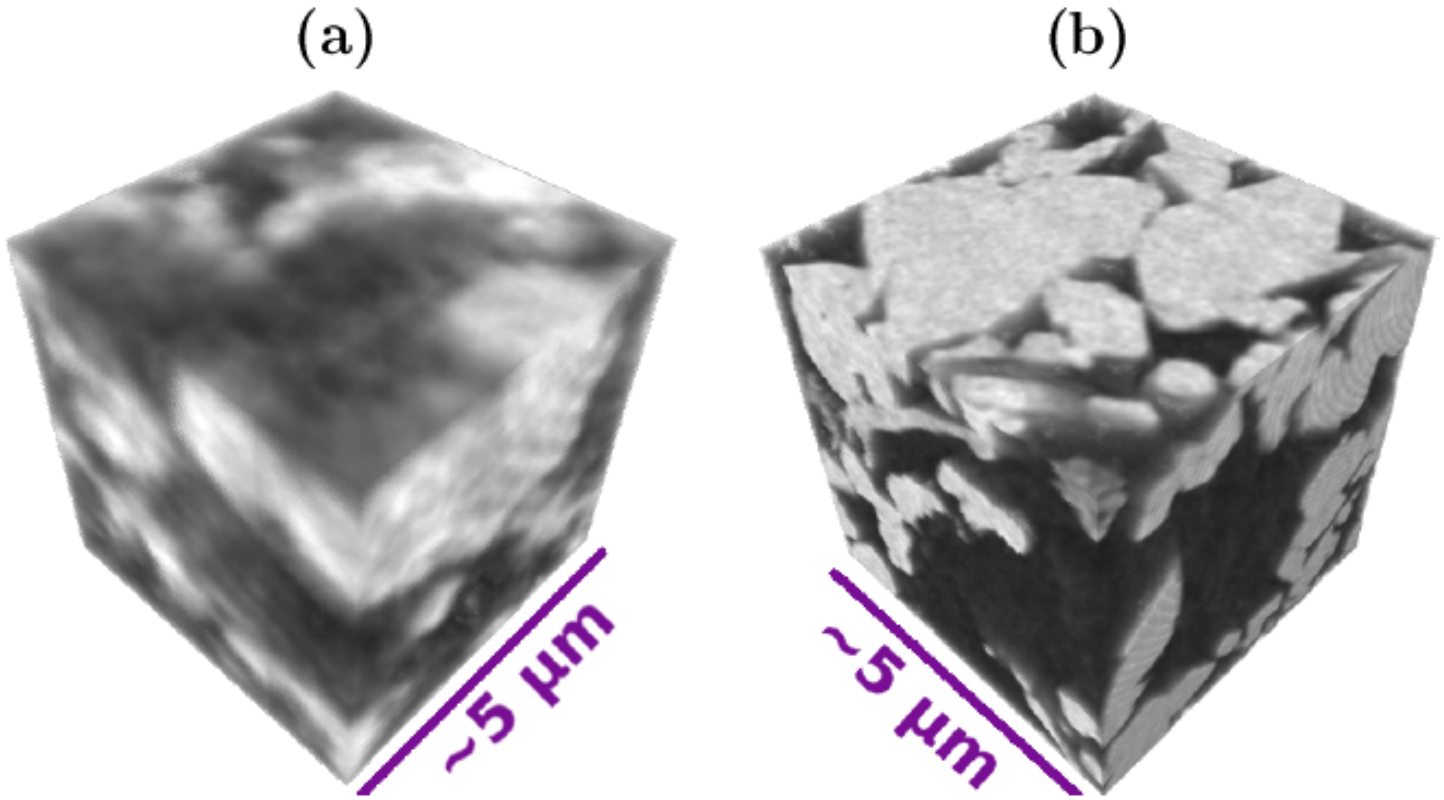

Figure 5: Examples of zooming in on regions in the CT-images for the two 3D chalk samples. To the left limestone (a) and to the right Aalborg chalk (b). Black ($Z = 1$) voxels constitutes the pore domain (assumed to be filled with brine). White ($Z = 0$) voxels represents regions of homogenous chalk. Aalborg chalk (b) contains a more complex pore morphology and was imaged with ptychographic X-ray nanotomography, which explains the sharper image compared to (a). Since the side length of the full samples are in the order of $N\Delta r \simeq 25$ µm (Table 2), the subvolumes shown here represents only about 1% of the chalk sample domains in our calculations.

Nuclear Magnetic Resonance

NMR important tool in modern technology.

Mobile Ex Situ High Resolution NMR

APPLICATIONS:

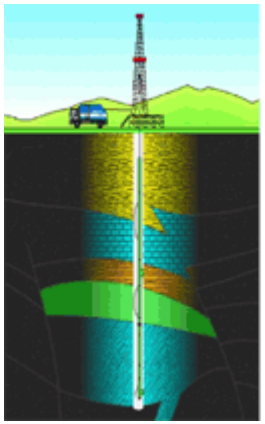

- Industrial sensing
- Oil well logging
- Medical imaging for large subjects
- Spectroscopy
- Imaging subjects or objects with ferromagnetic components
- Cargo inspection
- Stand-off detection

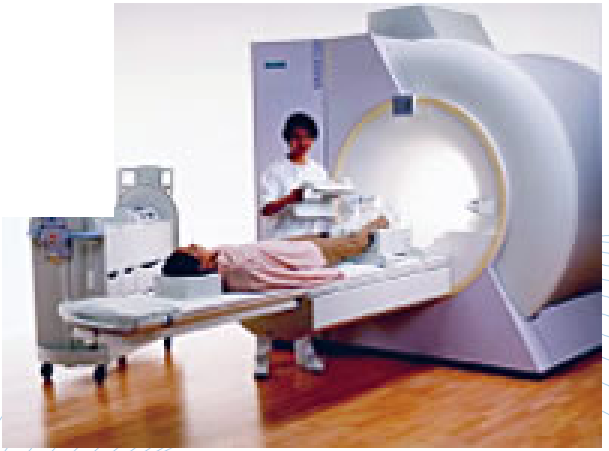

After simplifications of Bloch's equations

for NMR dynamics, we are left with a

reaction-diffusion equation

$$\frac{\partial M}{\partial t} = D_0 \nabla^2 M - \frac{M}{T_V},$$

with Robin boundary conditions

$$D_0 \mathbf{n} \cdot \nabla M + \rho M = 0.$$

We integrate out the spatial degrees

$$\mathcal{M}(t) = \int_{\Omega} M(\mathbf{x}, t)\, d\mathbf{x}$$

to obtain a time-dependent *total magnetization*

For uniform initial conditions, Gauss' theorem can provide the short time asymptote

$$\frac{1}{\mathcal{M}(0)} \left. \frac{d\mathcal{M}(t)}{dt} \right|_{t=0} = -\frac{\rho_0 S}{V}$$

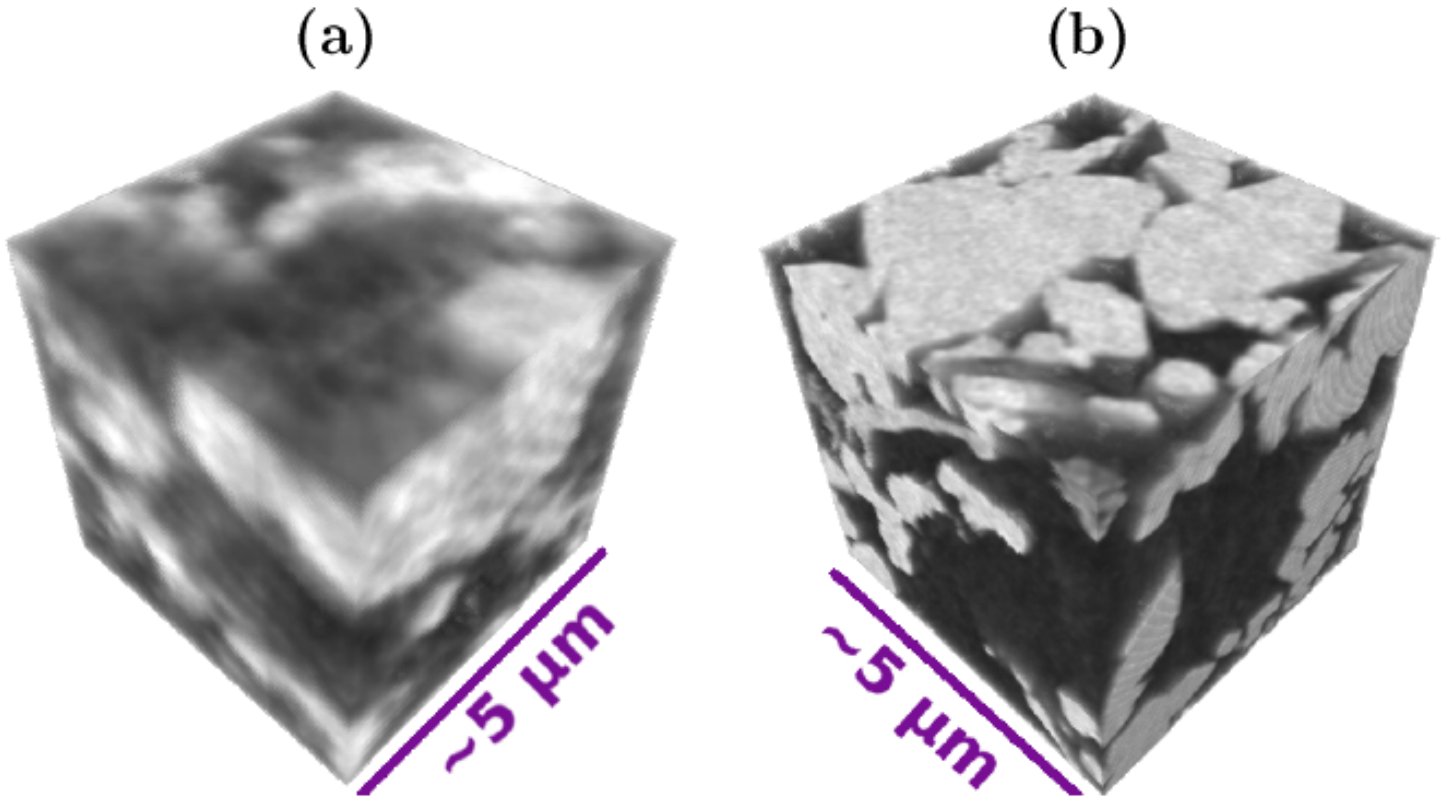

Figure 5: Examples of zooming in on regions in the CT-images for the two 3D chalk samples. To the left limestone (a) and to the right Aalborg chalk (b). Black ($Z = 1$) voxels constitutes the pore domain (assumed to be filled with brine). White ($Z = 0$) voxels represents regions of homogenous chalk. Aalborg chalk (b) contains a more complex pore morphology and was imaged with ptychographic X-ray nanotomography, which explains the sharper image compared to (a). Since the side length of the full samples are in the order of $N\Delta r \simeq 25$ µm (Table 2), the subvolumes shown here represents only about 1% of the chalk sample domains in our calculations.

In many applications the domain can be problematic…

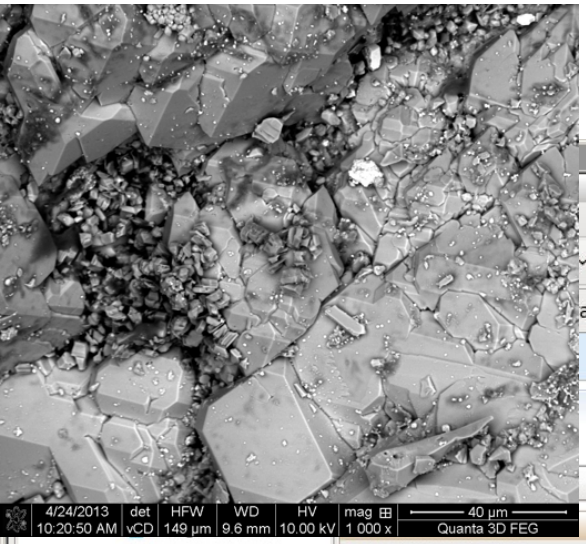

Boundary System 1
View 1
Geometry 1
Import 1 *(imp1)*
Form Union *(fin)*
Materials
Laplace Equation *(lpe*
Laplace Equation 1
Zero Flux 1
Initial Values 1
Dirichlet Boundary
Dirichlet Boundary

A problem occurred when building mesh feature 'Free Tetrahedral 1'.

Failed to generate mesh for domain.
- Domain: 1
Internal error in boundary respecting.
- x-coordinate: -0.5
- y-coordinate: 2
- z-coordinate: 21.1667

OK

Graphics

Messages | Progress | Log

Imported 1 geometry objects from /zhome/16/7/66472/ngs/32_32_32_pores_only.stl.

Dokument1 - Mic...
Arkiv Redigera Visa
Infoga Format Verktyg
Tabell Fönster Hjälp
Adobe PDF
Acrobat Comments
150%

1.96 GB | 5.93 GB

Start
SV 12:21

Try a random approach!

1.3.3. Random walk method (*RWM*). The RWM can be applied to find the local solution of *second-order* partial differential equations of the form

$$\frac{\partial u(\mathbf{x},t)}{\partial t} = \sum_{i=1}^{d} \alpha_i(\mathbf{x}) \frac{\partial u(\mathbf{x},t)}{\partial x_i} + \frac{1}{2} \sum_{i,j=1}^{d} \beta_{ij}(\mathbf{x}) \frac{\partial^2 u(\mathbf{x},t)}{\partial x_i \, \partial x_j} + q(\mathbf{x},t)\, u(\mathbf{x},t) + p(\mathbf{x},t) \qquad (6)$$

where α_i, β_{ij} are real-valued functions defined on $\Re^d$, $d \geqslant 1$ is an integer, and q, p denote real–valued functions defined on $\Re^d \times [0,\infty)$. The domain of definition of Equation (6) is $D \times (0,\infty)$, where $D \subset \Re^d$ is an open bounded set. The solution $u : D \times (0,\infty) \to \Re$ depends on the initial and boundary conditions that need to be specified. The operator of Equation (6) includes a large number of interesting special cases; for example, parabolic, hyperbolic, elliptic partial differential equations in $\Re^2$ correspond to the steady–state version of Equation (6) with $d = 2$ and $\beta_{12}(\mathbf{x})\,\beta_{12}(\mathbf{x}) - \beta_{11}(\mathbf{x})\,\beta_{22}(\mathbf{x}) = 0; > 0; < 0$, respectively. Therefore, for example, the Laplace, Poisson and Helmholtz equations are special cases of Equation (6).

The RWM method can be applied to find the local solution of Equation (6) with Dirichlet and/or Neumann boundary conditions. The solution by this method involves three steps. *First*, a diffusion process $\mathbf{X}$ with generator coinciding with the differential operator of Equation (6) has to be constructed. *Second*, a relationship needs to be established between the value of the unknown function u at $(\mathbf{x},t) \in D \times (0,\infty)$, the boundary conditions, and an expectation depending on the sample paths of $\mathbf{X}$. Properties of diffusion processes, features of stochastic integrals, and Itô's formula can be used to obtain this relationship. *Third*, a Monte Carlo algorithm needs to be developed to estimate the expectation giving $u(\mathbf{x},t)$.

When discussing the convergence of a stochastic calculation we need to mention:

1) A large enough number of trajectories to obtain a statistically significant result;

2) A small enough step-size to explore the small scale geometry of the media. The latter issue is also directly connected to the resolution chosen for a digital media.

If conditions 1) and 2) are fulfilled, one can accuratelly simulate diffusion processes with Dirichlet ($\rho_0 \to \infty$) and Neumann ($\rho_0 \to 0$) boundary conditions in Eq. (4). However, for Robin boundary conditions we need to consider also a third point.

3) Probability based modeling of the surface relaxation, including:

3a) a correct (algorithm dependent) relation between the local probability for surface relaxation (p_a) and the function $\rho_0(\mathbf{x}, t)$;

3b) A local description of the surface area for a digital media.

3a) We have derived (first order) relation between parameters in PDE model and the RWM:

$$p_S = \Delta r \rho / D_0.$$

3b) We have constructed (first order) local boundary conditions that can be calculated "on the fly":

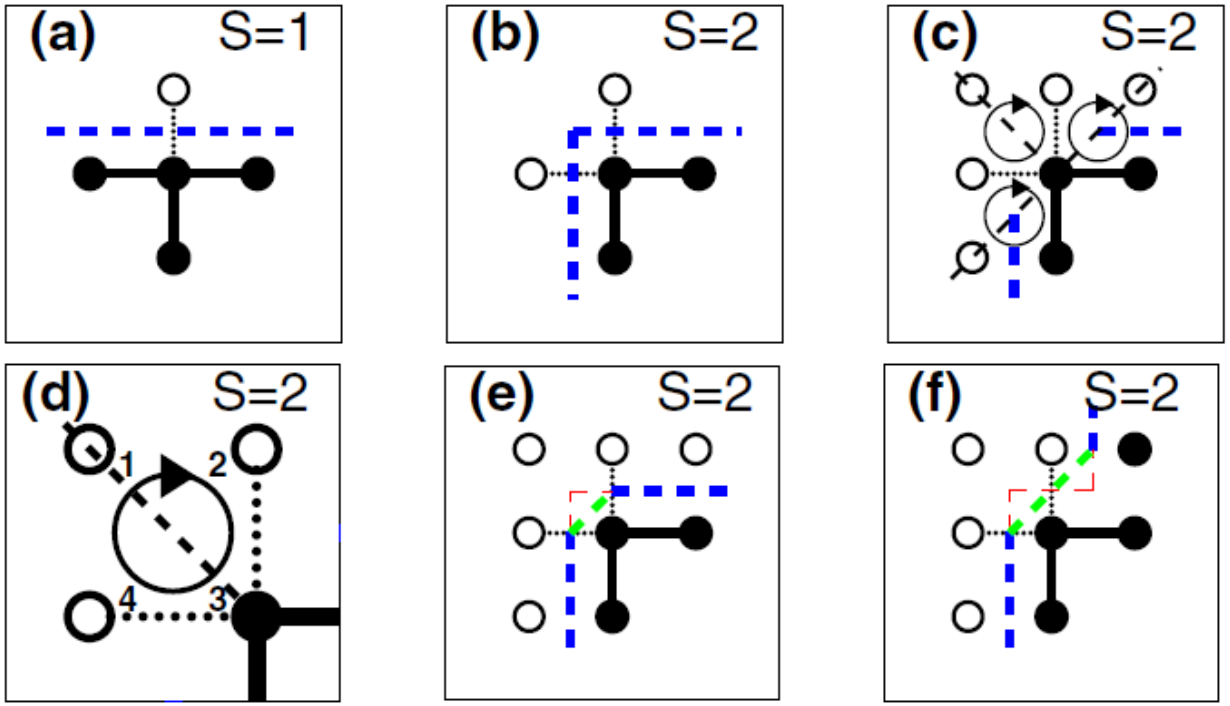

Above illustrated in 2D, generalized to any dimension.

In 2D the effects of ‘digitalization’ is easy to illustrate and quantify:

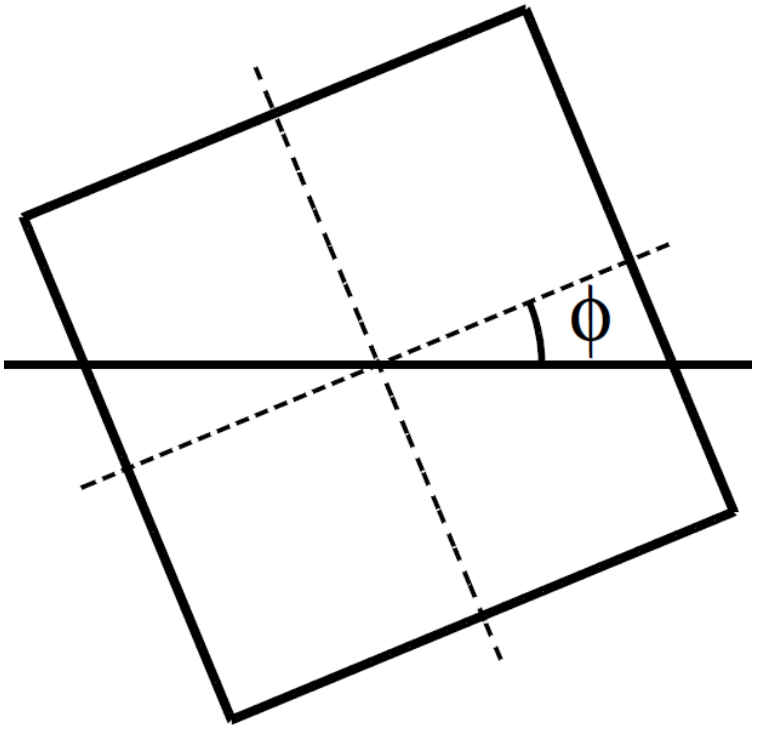

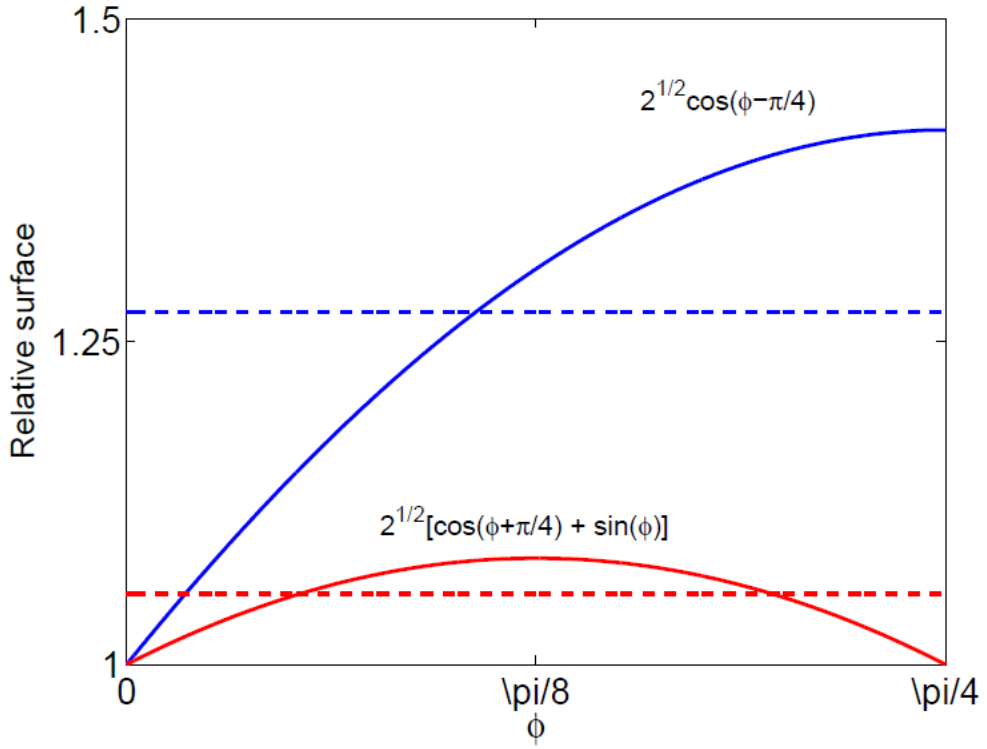

Comparative FEM simulations in 2D.

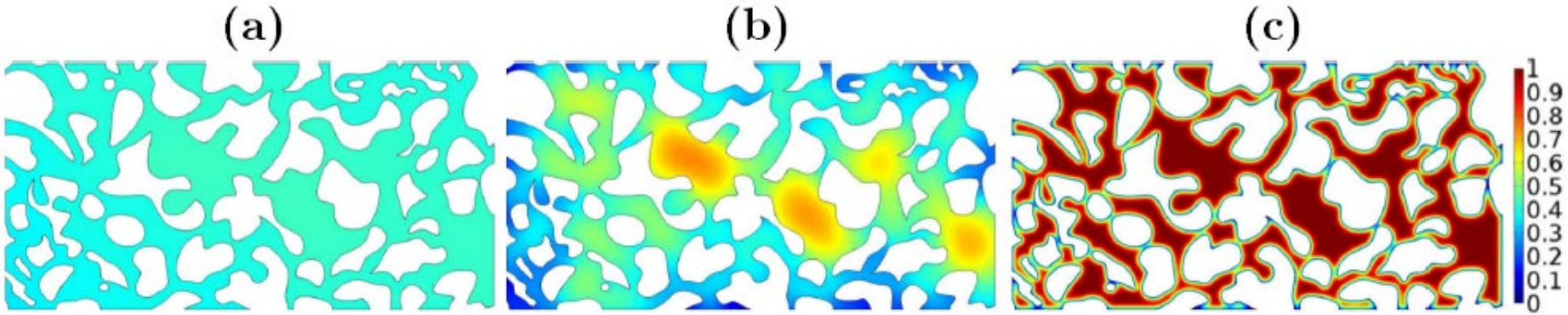

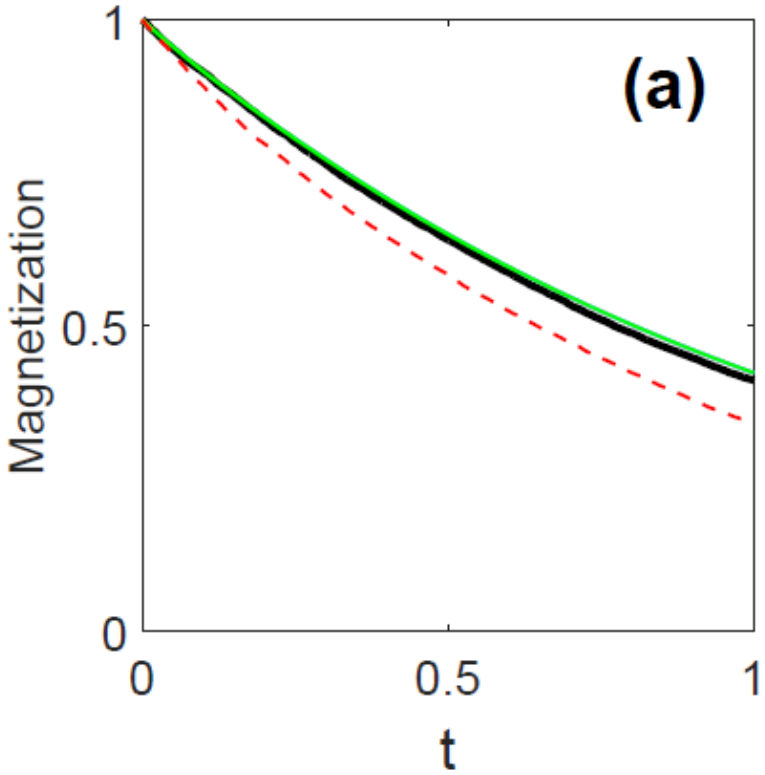

Comparison with analytic formulae: *Ball*

$$\mathcal{M}(t) = \mathcal{M}(0)\, 12 \sum_{j=1}^{\infty} \frac{\left[\sin\left(\sqrt{\lambda_j}\right) - \sqrt{\lambda_j}\cos\left(\sqrt{\lambda_j}\right)\right]^2}{\lambda_j^{3/2}\left[2\sqrt{\lambda_j} - \sin\left(2\sqrt{\lambda_j}\right)\right]} \exp\left(-\frac{D_0}{R_0^2}\lambda_j t\right), \quad (8)$$

where the eigenvalues λ_j are solutions of the equation $1 - \sqrt{\lambda_j}\cot\left(\sqrt{\lambda_j}\right) = R_0\rho/D_0$.

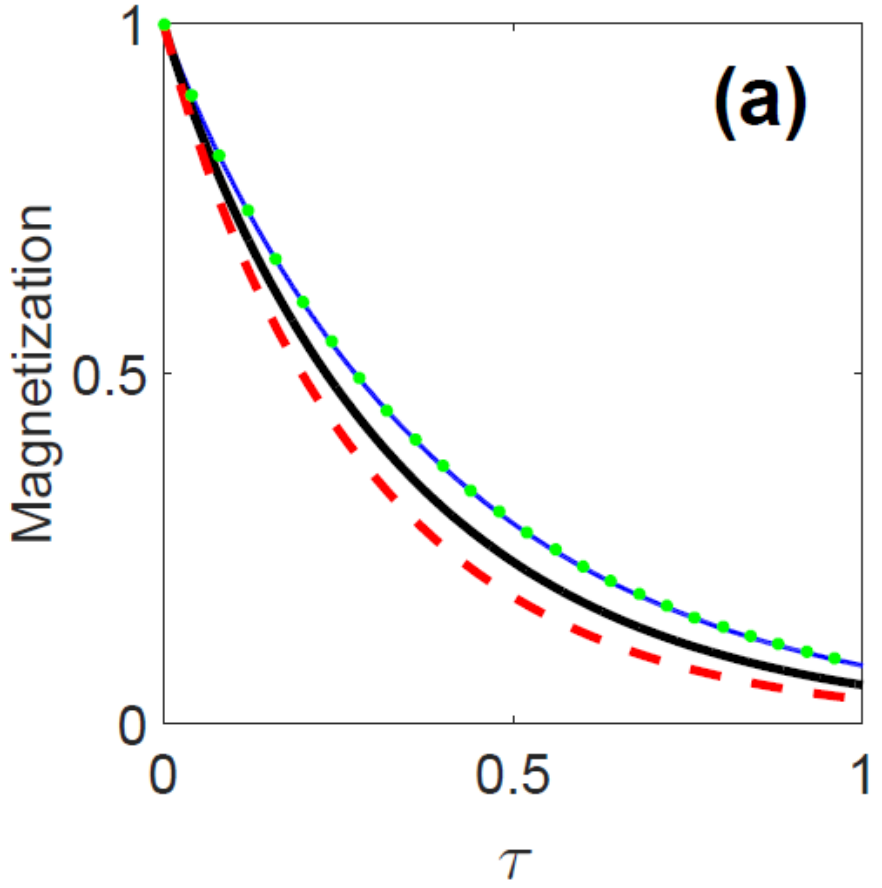

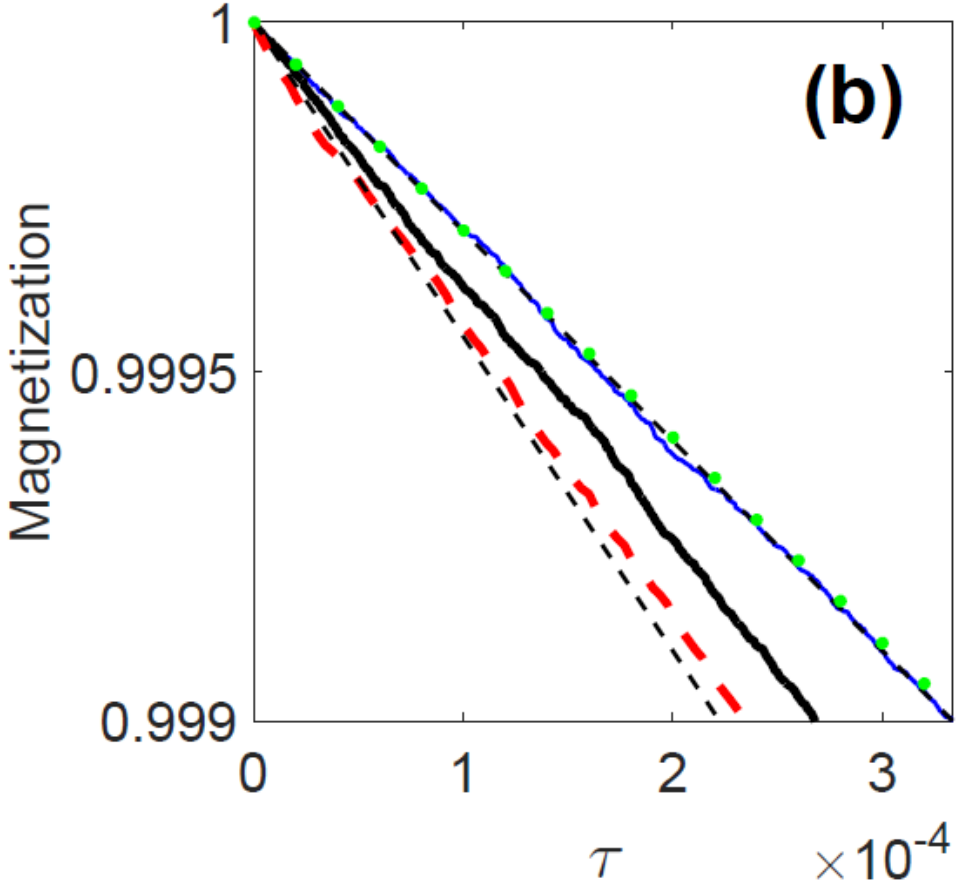

Comparison with analytic formulae: *Cube*

$$\mathcal{M}(t) = \mathcal{M}(0)\, 8 \left[\sum_{j=1}^{\infty} \frac{\sin^2\left(\sqrt{\lambda_j}\right)}{\sqrt{\lambda_j}\sin\left(\sqrt{\lambda_j}\right)\cos\left(\sqrt{\lambda_j}\right) + \lambda_j} \exp\left(-\frac{D_0}{R_0^2} \lambda_j t \right) \right]^3, \quad (9)$$

where the eigenvalues λ_j are solutions of the equation $\sqrt{\lambda_j}\tan\left(\sqrt{\lambda_j}\right) = R_0\rho/D_0$.

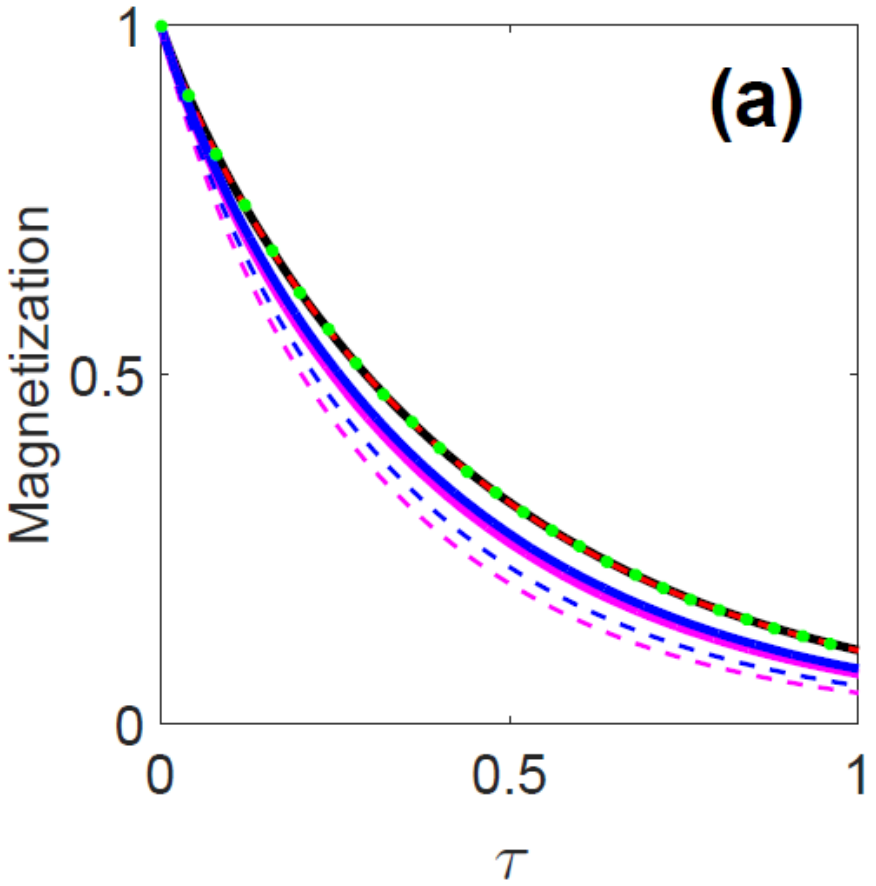

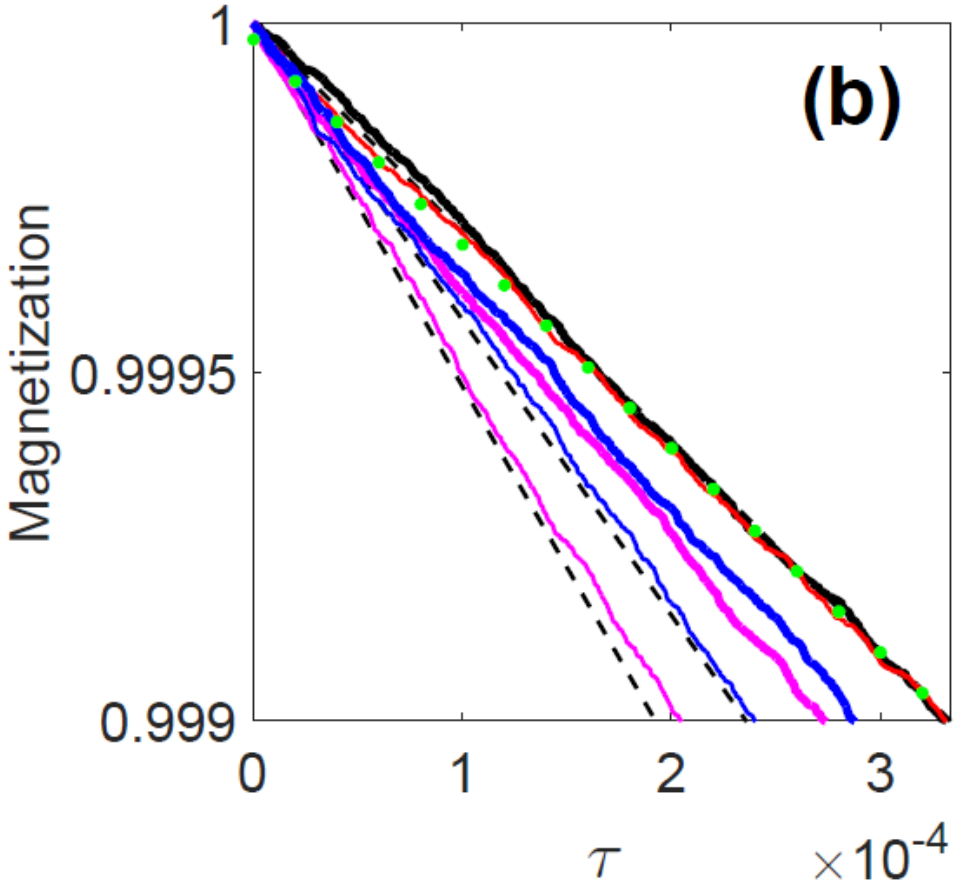

Simulations on 3D tomography images of chalk with a size in the order of $10^3 \times 10^3 \times 10^3$ voxels and resolution 10 nm

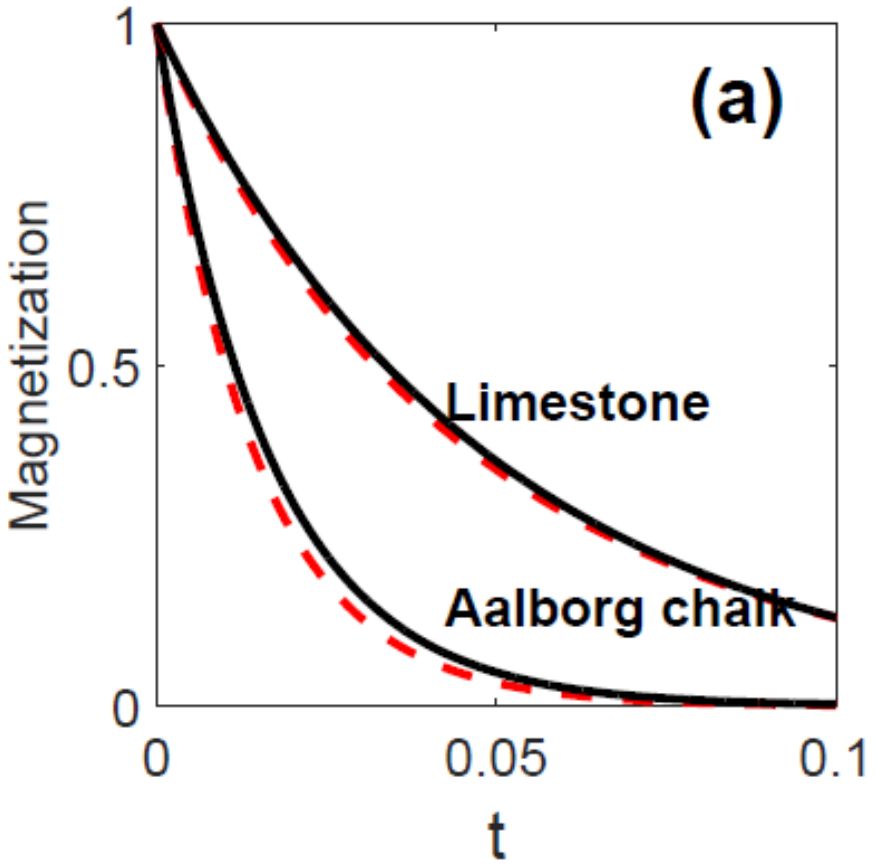

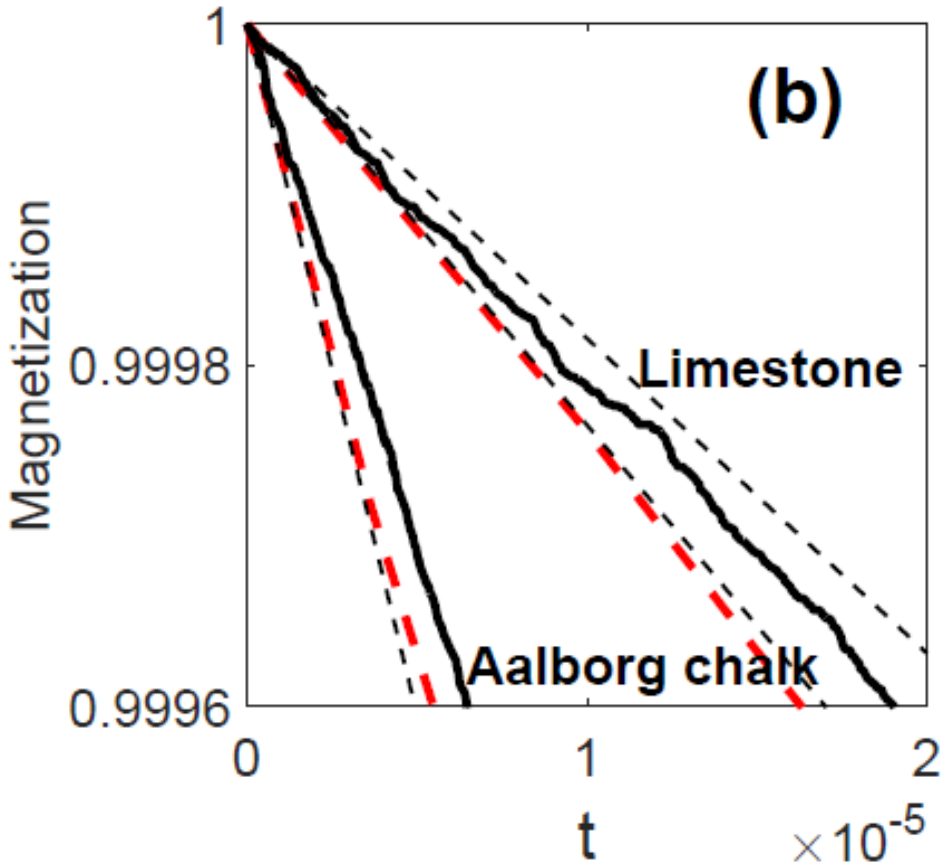

5. Discussion and summary

For the NMR relaxation simulation described here, we started from a deterministic partial differential equation and then used an equivalent stochastic particle formulation for the calculation. As expected from the previous investigation [15], the systematic errors for the NMR relaxation caused by the digitalisation of the 2D surfaces within the 3D geometrical objects occurs qualitatively different depending on the object and its orientation in relation to the coordinate system in a digital image. Here we have quantified those systematic errors and showed how they can be reduced for the ball and the cube in 3D and for an artificial 2D porous media for which comparative finite element calculations were tractable.

For two complex digital domains representing different chalk samples, that had similar porosity, but with substantially different specific area, we found qualitatively different relaxation dynamics. Additionally for each of those complex domains the relaxation curve without local boundary conditions were markably lower and we expect to have removed a major part of the errors between the true NMR relaxation and its simulated dynamics.

Stefan-problem

2 The Stefan problem in one dimension

In our model for the one-dimensional Stefan problem we consider a block of ice with infinite extent and one surface to air. At $t = 0$ there is no water phase and the ice phase is at $T_{ice} = 0°$. But for $t > 0$ the ice has started melting and thus we have a water phase on top of the ice. The temperature of the surface, i.e. the interface between air and water for $t > 0$ is changing over time according to $f(t)$ and to simulate a melting process, we assume $f(t) \geq 0 \ \forall t$. This yields the following equations:

$$\frac{\partial T}{\partial t} = \alpha_L \frac{\partial^2 T}{\partial x^2}\,, \qquad 0 < x < s(t)\,, \qquad t > 0\,, \tag{2.1}$$

$$T(0,t) = f(t)\,, \qquad t > 0\,, \tag{2.2}$$

$$T(x,0) = 0\,, \tag{2.3}$$

$$l\rho \frac{ds}{dt} = -k_L \left.\frac{\partial T}{\partial x}\right|_{x=s(t)}\,, \qquad t > 0\,, \tag{2.4}$$

$$s(0) = 0\,, \tag{2.5}$$

$$T(s(t),t) = T_M = 0\,, \qquad t > 0\,. \tag{2.6}$$

Stefan-problem

The analytical solution to the problem when $f(t) = T_0$ is (see e.g. [3])

$$\begin{cases} T(x,t) & = T_0 \left(1 - \frac{\operatorname{erf}(x/(2\sqrt{\alpha_L t}))}{\operatorname{erf}(\lambda)}\right) \\ s(t) & = 2\lambda\sqrt{\alpha_L t} \\ \beta\sqrt{\pi}\lambda e^{\lambda^2}\operatorname{erf}\lambda & = T_0\,, \end{cases} \tag{2.8}$$

where $\beta = c_L/l$ and $\operatorname{erf}(x)$ is the *error function* defined as $\frac{2}{\sqrt{\pi}}\int_0^x e^{-y^2}\,dy$. A special case when an analytical solution also can be found is when $f(t) = e^t - 1$. We will use this for comparison with our RWM in the result section. Provided $\beta = 1$, the solution is [9]

$$\begin{cases} T(x,t) & = e^{t-x} - 1 \\ s(t) & = t\,. \end{cases} \tag{2.9}$$

Stefan-problem

Modelling of the moving boundary

Each walker carries an amount of heat that moves the boundary a step Δs.

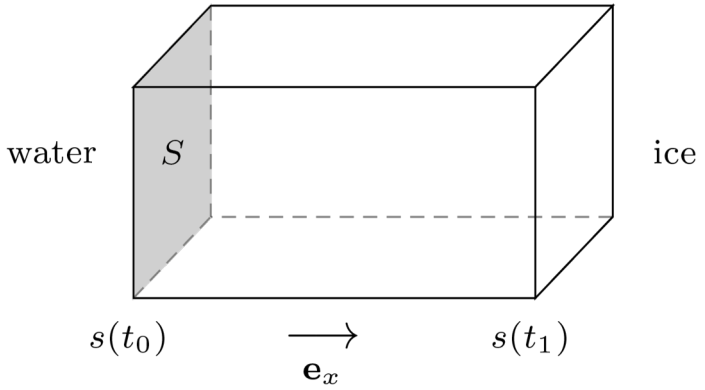

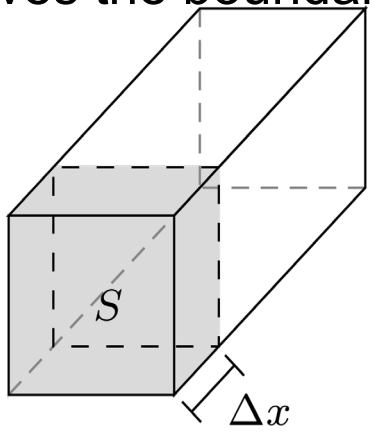

$$Q = V \cdot \rho \cdot l = S(s(t_1) - s(t_0)) \cdot \rho l$$

$$Q_{walker} = c \cdot \rho \cdot V \cdot 1°\mathrm{C} = c \cdot \rho \cdot \Delta x \cdot S \cdot 1°\mathrm{C}$$

$$\Delta s = \frac{c\rho \Delta x S}{\rho l S} = \frac{c}{l}\Delta x\,.$$

$$\frac{\Delta s}{n} \ll \Delta x\,.$$

Stefan-problem

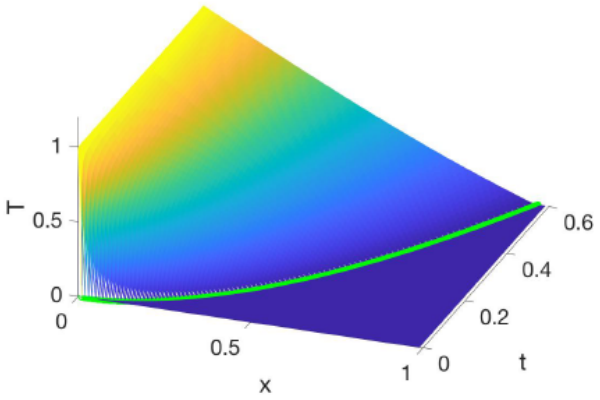

(a) *Analytical solution from (2.8).*

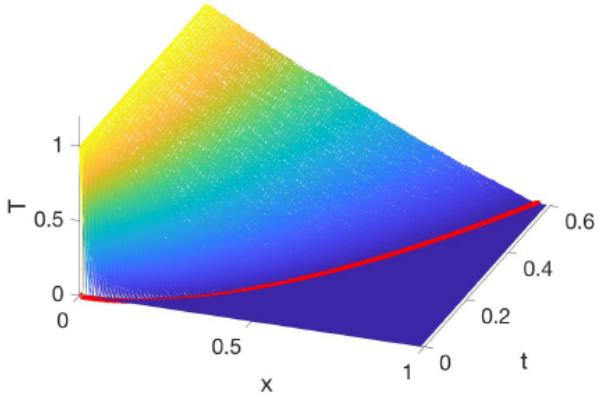

(b) *RWM solution with* $n = 10^4$ *and* $\Delta x = 0.01$.

Figure 4.3: Solutions for Stefan problem with boundary condition $f(t) = 1$ *for* $t \in [0, 1]$.

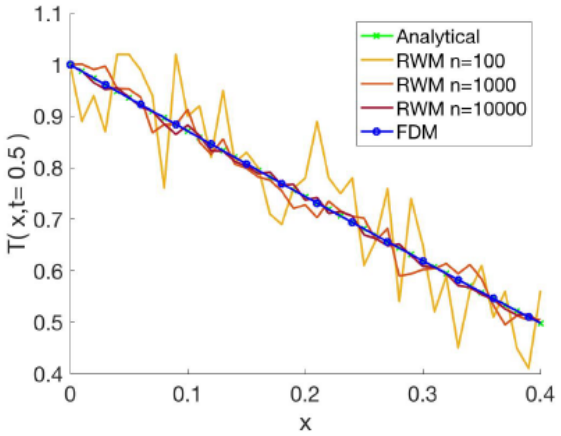

(a) *RWM solutions with* $\Delta x = 0.01$ *and different number of iterations* n, *FDM and analytical solutions,* $x \in [0, 0.4]$.

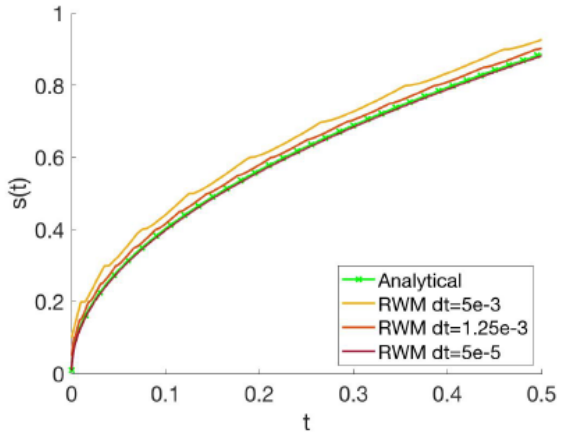

(b) *Solution for the moving boundary* $s(t)$ *with analytical values and RWM for* $n = 10^4$ *and different step lengths* Δt, $t \in [0, 0.3]$.

Figure 4.4

Stefan-problem

Results for BC: e^t-1

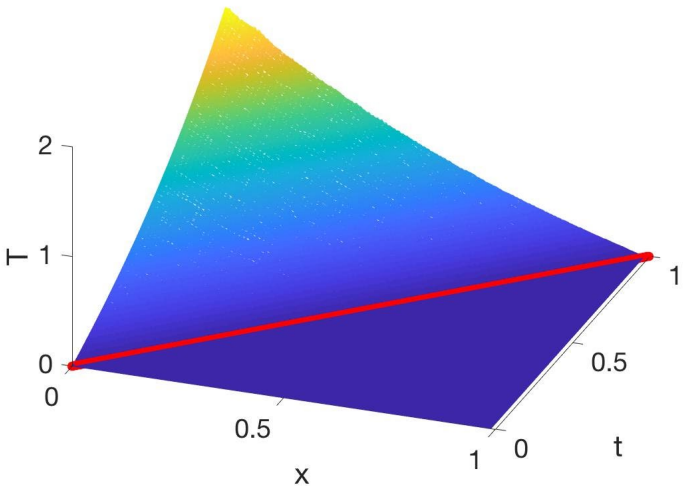

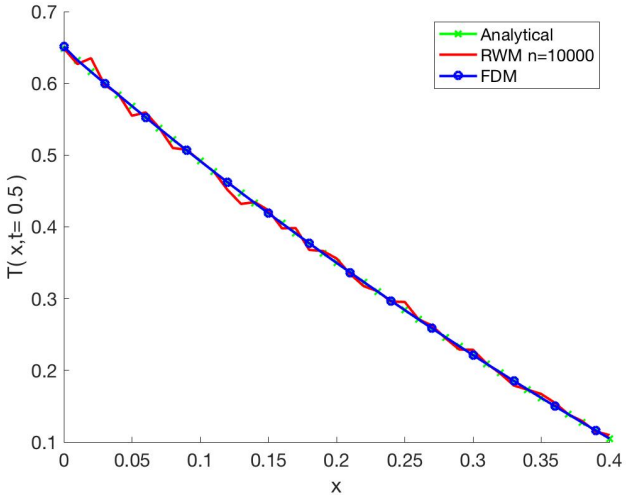

$$\frac{\partial T}{\partial t} = \alpha_L \frac{\partial^2 T}{\partial x^2},$$

$$T(0,t) = \text{e^t-1}$$

$$T(x,0) = 0,$$

$$l\rho \frac{ds}{dt} = k_L \left.\frac{\partial T}{\partial x}\right|_{x=s(t)},$$

$$s(0) = 0,$$

$$T(s(t),t) = T_M = 0,$$

Stefan-problem

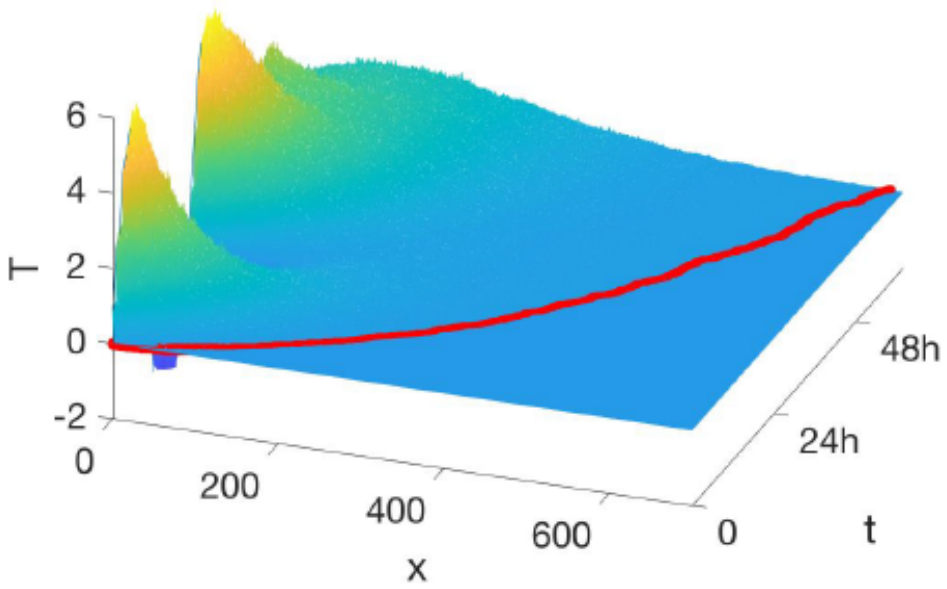

Figure 4.9: RWM model where $f(t)$ is set to observed day temperatures at Örebro airport 1-3 March 2019. x in mm and $t \in [0, 62\,h]$.

Thank you!

ÖREBRO UNIVERSITET

Interested to read more:

Ögren, M. (2014). Local boundary conditions for NMR-relaxation in digitized porous media. *The European Physical Journal B*, 87 (11), 255. (arXiv:1312.6581)

Ögren, M. , Jha, D. , Dobberschütz, S. , Müter, D. , Carlsson, M. , Gulliksson, M. , Stipp, S. & Sørensen, H. (2019). Numerical simulations of NMR relaxation in chalk using local Robin boundary conditions.
Journal of magnetic resonance, 308. (arXiv:1909.09618)

A random walk method for the heat equation with moving boundary.
Andreas Lockby, Bachelor thesis 2016:
http://oru.diva-portal.org/smash/record.jsf?pid=diva2%3A935914&dswid=3345

Solution of the Stefan problem with general time-dependent boundary conditions using a random walk method. Daniel Stoor, Bachelor thesis 2019:
http://uu.diva-portal.org/smash/record.jsf?pid=diva2%3A1325632&dswid=-6545